Die Pharmazie

Pharmazie **2026**; 81(7): 51570
https://doi.org/10.31083/Pharmazie51570

Research Article

Entinostat and Tucidinostat Potentiate Temozolomide Response in Glioblastoma Models

Ruijie Chen[1], Junhui Su[1], Xinjue Dong[1], Xinyi Tang[1], Yuqi Yang[1], Qingquan Li[1,*]

[1]Department of Pharmacology, School of Pharmaceutical Sciences, Fudan University, 200120 Shanghai, China
*Correspondence: 061101040@fudan.edu.cn (Qingquan Li)
Academic Editors: Daniel J. V. A. dos Santos and Walter E. Müller
Submitted: 6 March 2026 Revised: 12 June 2026 Accepted: 25 June 2026 Published: 24 July 2026

Abstract

Background: Glioblastoma (GBM) frequently develops resistance to temozolomide (TMZ), limiting the effectiveness of standard therapy. Histone deacetylase (HDAC) inhibitors have emerged as potential chemosensitizers; however, the comparative performance of these inhibitors and the associated mechanistic impact remain incompletely characterized. **Methods:** *In vitro*, this study systematically evaluated the effects of the Class I-selective HDAC inhibitors Entinostat and Tucidinostat, and the pan-HDAC inhibitor Vorinostat on TMZ sensitivity in multiple GBM cell lines (U87, U251, LN229). Additionally, this study assessed cell viability, morphology, and the expression of selected markers glial fibrillary acidic protein (GFAP), microtubule-associated protein 2 (MAP2), class III β-tubulin (TUBB3), and synapsin I (SYN1). *In vivo*, the therapeutic efficacy of Entinostat combined with TMZ was evaluated in a U87 xenograft mouse model by measuring tumor growth, and the expression of GFAP and TUBB3 was examined in tumor tissues. Clustered Regularly Interspaced Short Palindromic Repeats associated protein 9 (CRISPR-Cas9)-mediated knockout of HDAC1/2/3 was used to test the dependence of these effects on canonical Class I HDACs. **Results:** Entinostat and Tucidinostat significantly enhanced TMZ-induced cytotoxicity across all cell lines, demonstrating greater TMZ-sensitizing activity than Vorinostat under the conditions tested. Treatment was associated with altered cell morphology and changes in marker expression, including reduced GFAP and increased MAP2 and TUBB3. In the U87 xenograft model, Entinostat combined with TMZ significantly suppressed tumor growth and was associated with decreased GFAP and increased TUBB3 expression. Importantly, both TMZ sensitization and the associated morphological and marker changes persisted in HDAC1/2/3-knockout cells, suggesting that the effects are not fully explained by HDAC1/2/3 depletion. These effects were consistent across multiple cell lines and in xenograft tumors. **Conclusions:** Entinostat and Tucidinostat enhance TMZ sensitivity in GBM models and are associated with specific markers and morphological changes that persist despite HDAC1/2/3 knockout. These findings support further evaluation of Entinostat and Tucidinostat as TMZ-sensitizing agents in GBM models and highlight associated phenotypic and molecular changes that warrant further mechanistic validation.

Keywords: glioblastoma; histone deacetylase inhibitors; temozolomide; drug resistance

1. Introduction

Glioblastoma (GBM) is the most common and aggressive primary malignant tumor of the central nervous system in adults. Classified by the World Health Organization (WHO) as Grade IV glioma, GBM exhibits extreme malignancy and poor patient prognosis, with a global five-year survival rate below 10% and an incidence of approximately 6 cases per 100,000 individuals annually [1,2,3,4]. GBM accounts for ~55% of all gliomas and remains incurable despite current multimodal therapy, which consists of maximal safe surgical resection followed by radiotherapy with concomitant and adjuvant temozolomide (TMZ) chemotherapy [5,6,7]. Although TMZ extends median survival to ~15 months, its long-term benefit is undermined by the emergence of chemoresistant tumor cell populations that drive recurrence [6,8,9].

Resistance to TMZ is shaped by diverse molecular and epigenetic mechanisms, including elevated expression of the DNA repair enzyme O^6-methylguanine-DNA methyltransferase (MGMT), activation of the DNA damage response (DDR), and chromatin remodeling events [10,11,12,13,14]. Among the epigenetic regulators, histone deacetylases (HDACs) have attracted particular interest due to their pivotal role in transcriptional repression, cell cycle control, and tumor progression [15]. By removing acetyl groups from lysine residues on histone proteins, HDACs compact the chromatin structure and silence gene transcription, thereby fostering GBM cell proliferation, suppressing apoptosis, and enhancing invasive behavior [16,17].

Recent studies have identified Class I HDACs (HDAC1, HDAC2, and HDAC3) not only as key drivers of GBM malignancy, but also as potential modulators of chemoresistance. Elevated expression of these enzymes has been linked to poor patient prognosis, enhanced DNA repair capacity, and the maintenance of tumor-initiating cell populations [18,19]. Pharmacological blockade of HDAC1/2/3 can alter GBM transcriptional programs, reduce clonogenic growth, and in some contexts, sensitize tumor cells to TMZ [20]. Traditionally, HDAC inhibition in GBM has relied on broad-spectrum agents such as the hydroxamic acid Vorino-

stat. However, the pan-HDAC activity of these agents can trigger off-target effects or undesired toxicities, complicating clinical translation [21,22]. In contrast, Entinostat and Tucidinostat are reported to specifically inhibit Class I HDACs and have been explored in cancer-related settings [23].

The present study compared the TMZ-sensitizing effects of Entinostat and Tucidinostat with those of the broad-spectrum hydroxamic acid inhibitor Vorinostat. Guided by our *in vitro* and *in vivo* findings, we further sought to explore the involvement of HDAC1/2/3 in mediating these effects using Clustered Regularly Interspaced Short Palindromic Repeats associated protein 9 (CRISPR-Cas9) knockout GBM models. Entinostat and Tucidinostat were found to enhance TMZ cytotoxicity and were associated with treatment-related marker and morphological changes in GBM cells. These effects persisted even in the absence of HDAC1/2/3, suggesting that HDAC1/2/3 depletion alone did not fully account for the observed responses. The current observations provide novel insights that warrant further mechanistic evaluation in more clinically relevant models of GBM.

2. Materials and Methods

2.1 Cell Culture and Drug Treatments

All cell lines were validated by STR profiling and tested negative for mycoplasma. The human GBM cell lines U-87 MG (U87; ATCC, HTB-14), U-251 MG (U251; Mcellbank, M-C1196), and LN-229 (LN229; ATCC, CRL-2611) were cultured in Dulbecco's Modified Eagle Medium (DMEM; Gibco) supplemented with 10% fetal bovine serum (FBS; Gibco) and 1% penicillin–streptomycin (Viva-Cell). Cultures were maintained in a humidified incubator at 37 °C with 5% CO_2. Temozolomide (TMZ; MedChemExpress) was stored as a powder at –80 °C. For experimentations, TMZ was dissolved in dimethyl sulfoxide (DMSO; Solarbio) and diluted in complete medium to final concentrations of 100–2000 µM. Treatment durations were 48 h or 72 h as specified. Entinostat, Tucidinostat, and Vorinostat (all from MedChemExpress) were stored as powders at –80 °C and prepared as stock solutions in DMSO. For combination treatments with TMZ, HDAC inhibitors were used at a final concentration of 1 µM for 48 h or 72 h.

2.2 Cell Viability Assay

Cells were seeded into 96-well plates at 1000 cells/well in 100 µL of medium and allowed to adhere for 24 h. The medium was then replaced with fresh medium containing the indicated drugs. Cell viability was measured using the Cell Counting Kit-8 (CCK-8; C0038, Beyotime Biotechnology, Shanghai, China) according to the manufacturer's instructions. Briefly, 100 µL of fresh medium containing 10% CCK-8 reagent was added to each well, incubated at 37 °C for 1 h, and the absorbance at 450 nm was measured with a Multiskan FC microplate reader (Thermo Fisher Scientific). Assays were performed in triplicate, and viability was expressed as a percentage of vehicle (DMSO) controls.

2.3 Quantitative Reverse Transcription Polymerase Chain Reaction (qRT-PCR)

Total RNA was isolated using the FastPure Cell/Tissue Total RNA Isolation Kit (RC112-01, Vazyme Biotech Co., Ltd., Nanjing, Jiangsu, China). RNA purity and concentration were assessed with a NanoDrop 2000 spectrophotometer (Thermo Fisher Scientific, Waltham, MA, USA). Reverse transcription was performed using HiScript III RT SuperMix for qPCR (+gDNA wiper; R323-01, Vazyme Biotech Co., Ltd., Nanjing, Jiangsu, China). Quantitative PCR was performed with ChamQ Universal SYBR qPCR Master Mix (Q711-02, Vazyme Biotech Co., Ltd., Nanjing, Jiangsu, China) on the QuantStudio™ 3 Real-Time PCR System (Thermo Fisher Scientific, Waltham, MA, USA). Primer sequences are listed in **Supplementary Table 1**.

2.4 CRISPR-Cas9-Mediated Knockout of HDAC1/2/3

Single-guide RNAs (sgRNAs) targeting HDAC1, HDAC2, and HDAC3 were designed using the Broad Institute CRISPR design tool and cloned into the Lenti-CRISPRv2 vector (Addgene plasmid #52961) according to Ran et al. [24]. sgRNA sequences are listed in **Supplementary Table 2**. Lentiviral particles were generated by co-transfecting 293T cells with the sgRNA/Cas9 vector, psPAX2 packaging plasmid (12260, Addgene, Watertown, MA, USA), and pMD2.G envelope plasmid (12259, Addgene, Watertown, MA, USA) using Polyjet™ reagent (SL100688, SignaGen Laboratories, Frederick, MD, USA). Viral supernatants were collected and used to infect U87 and U251 cells in the presence of 2 µg/mL polybrene (Beyotime). Transduced cells were selected with puromycin (2 µg/mL; HY-B1743A, MedChemExpress (MCE), Monmouth Junction, NJ, USA) for 7 days to establish stable knockout pools. Knockout efficiency was validated by Western blotting.

2.5 Western Blotting

Cells were lysed in RIPA buffer (P0013B, Beyotime Biotechnology, Shanghai, China), and protein concentrations were determined using standard protocols. Lysates were denatured in Laemmli buffer, separated by SDS-PAGE (precast gels), and transferred to PVDF membranes (Millipore). Membranes were blocked with 5% nonfat milk (P0216, Beyotime Biotechnology, Shanghai, China) for 1 h at room temperature, incubated with primary antibodies overnight at 4 °C, and then with HRP-conjugated secondary antibodies for 1 h at room temperature. Antibodies are listed in **Supplementary Table 3**. Bands were visualized using an ECL detection system (Tanon).

2.6 Tumor Xenograft Experiments

All animal studies were approved by the Animal Ethics Committee of the School of Pharmacy, Fudan University, and were performed in accordance with institutional guidelines. Female BALB/c nude mice (4 weeks old) were purchased from Shanghai SLAC Laboratory Animal Co., Ltd. and housed under standard specific pathogen-free conditions with controlled temperature, humidity, and a 12 h light/dark cycle. For all tumor cell inoculation procedures, mice were anesthetized with isoflurane delivered via a precision vaporizer (induction at 4% and maintenance at 2% in oxygen). Adequate anesthesia was confirmed before the procedure by the absence of the pedal withdrawal reflex. U87MG cells (8×10^6 in 0.1 mL PBS) were injected subcutaneously into the right flanks of mice. When tumors reached ~100 mm^3, 24 mice were randomized into four groups (n = 6 per group): (1) Vehicle control: oral gavage with 0.5% CMC-Na (0.1 mL) plus intraperitoneal PBS (0.1 mL); (2) Entinostat: oral gavage with Entinostat (5 mg/kg in 0.5% CMC-Na, 0.1 mL) plus intraperitoneal PBS; (3) TMZ: oral gavage with 0.5% CMC-Na plus intraperitoneal TMZ (10 mg/kg in PBS, 0.1 mL); (4) Combination: oral gavage with Entinostat (5 mg/kg) plus intraperitoneal TMZ (10 mg/kg). Animals were distributed across cages to minimize cage effects. Treatments were administered every other day. Tumor volume was measured every 3 days using calipers and calculated as: volume = (length × $width^2$) / 2. At the study endpoint (day 33), mice were euthanized by cervical dislocation, and tumors were excised, weighed, photographed, fixed in 4% paraformaldehyde, and paraffin-embedded for histology. No animals were excluded from analysis. Outcome assessments were conducted in a blinded manner.

2.7 Immunofluorescence Staining

Paraffin sections were baked at 56 °C overnight, deparaffinized with xylene, and rehydrated through graded ethanol. Antigen retrieval was performed in Tris-EDTA buffer (1 mM, pH 9.0) using microwave heating (900 W for 2.5 min, then 150 W for 20 min). Sections were blocked with 5% goat serum (16210064, Gibco, Waltham, MA, USA) for 30 min, incubated overnight at 4 °C with primary antibodies (**Supplementary Table 3**), and then with Alexa Fluor–conjugated secondary antibodies (**Supplementary Table 3**) for 1 h at room temperature in the dark. Nuclei were counterstained with Hoechst staining solution (C1011, Beyotime Biotechnology, Shanghai, China), and slides were mounted in Anti-fade mounting medium (P0126, Beyotime Biotechnology, Shanghai, China) and imaged using Revolve Generation 2 epifluorescence microscope (ECHO, Inc., San Diego, CA, USA).

2.8 Statistical Analysis

Data analysis and visualization were performed using GraphPad Prism v10.3.1 (GraphPad Software, San Diego, CA, USA). Two-tailed Student's *t*-tests were used for comparisons between two groups. One-way analysis of variance (ANOVA) followed by Tukey's post-hoc test was used for multiple group comparisons. Two-way ANOVA was used for growth curve analysis. Data are presented as the mean ± SEM, and differences were considered statistically significant at $p < 0.05$.

3. Results

3.1 Entinostat and Tucidinostat Sensitize GBM Cells to TMZ More Effectively Than Vorinostat

Given that Entinostat and Tucidinostat selectively target Class I HDACs (HDAC1/2/3) whereas Vorinostat acts as broad-spectrum HDAC blockers, we first sought to compare their efficacy in enhancing GBM cell sensitivity to TMZ. To this end, we evaluated the combinatorial effects of Entinostat and Tucidinostat, and the pan-HDAC inhibitor Vorinostat across three human GBM cell lines (U251, U87, and LN229). For all combination studies, a sub-cytotoxic concentration (1 μM) of each inhibitor was used to minimize confounding effects from HDAC inhibitor-induced cell death (**Supplementary Fig. 1**). Cell viability assays demonstrated that co-treatment with Entinostat and Tucidinostat markedly potentiated TMZ cytotoxicity, as evidenced by a pronounced leftward shift in the TMZ dose-response curves compared with TMZ monotherapy. In contrast, Vorinostat did not produce a comparable sensitizing effect at 1 μM, with its combination curves largely overlapping those for TMZ alone. These patterns were consistently observed across U251 (Fig. 1A), U87 (Fig. 1B), and LN229 cells (Fig. 1C).

Quantification of TMZ IC_{50} values confirmed significant sensitization with the Class I-selective benzamide inhibitors, Entinostat and Tucidinostat, across all three GBM cell lines (Fig. 1D–F, **Supplementary Table 4**). Notably, both agents emerged as potent and consistent sensitizers in U251 and LN229 cells, with marked IC_{50} reductions relative to TMZ monotherapy. In contrast, the pan-HDAC inhibitor Vorinostat did not enhance TMZ sensitivity at the tested concentration, yielding IC50 values comparable to TMZ alone. Under the tested conditions, Entinostat and Tucidinostat produced more consistent TMZ sensitization than Vorinostat, providing a rationale for subsequent mechanistic studies.

We further performed a checkerboard combination assay using Entinostat and TMZ in U251 cells to address the pharmacological interaction between them (Fig. 1G). Chou–Talalay analysis revealed CI values of 0.6474, 0.5913, and 0.5829 at Fa values of 0.50, 0.75, and 0.90, respectively (Fig. 1H). All were <1, indicative of synergistic drug interactions. These results provide quantitative evidence that the enhanced TMZ response induced by Entinostat cannot be solely attributed to additive cytotoxicity and instead reflects a true synergistic interaction between the two agents.

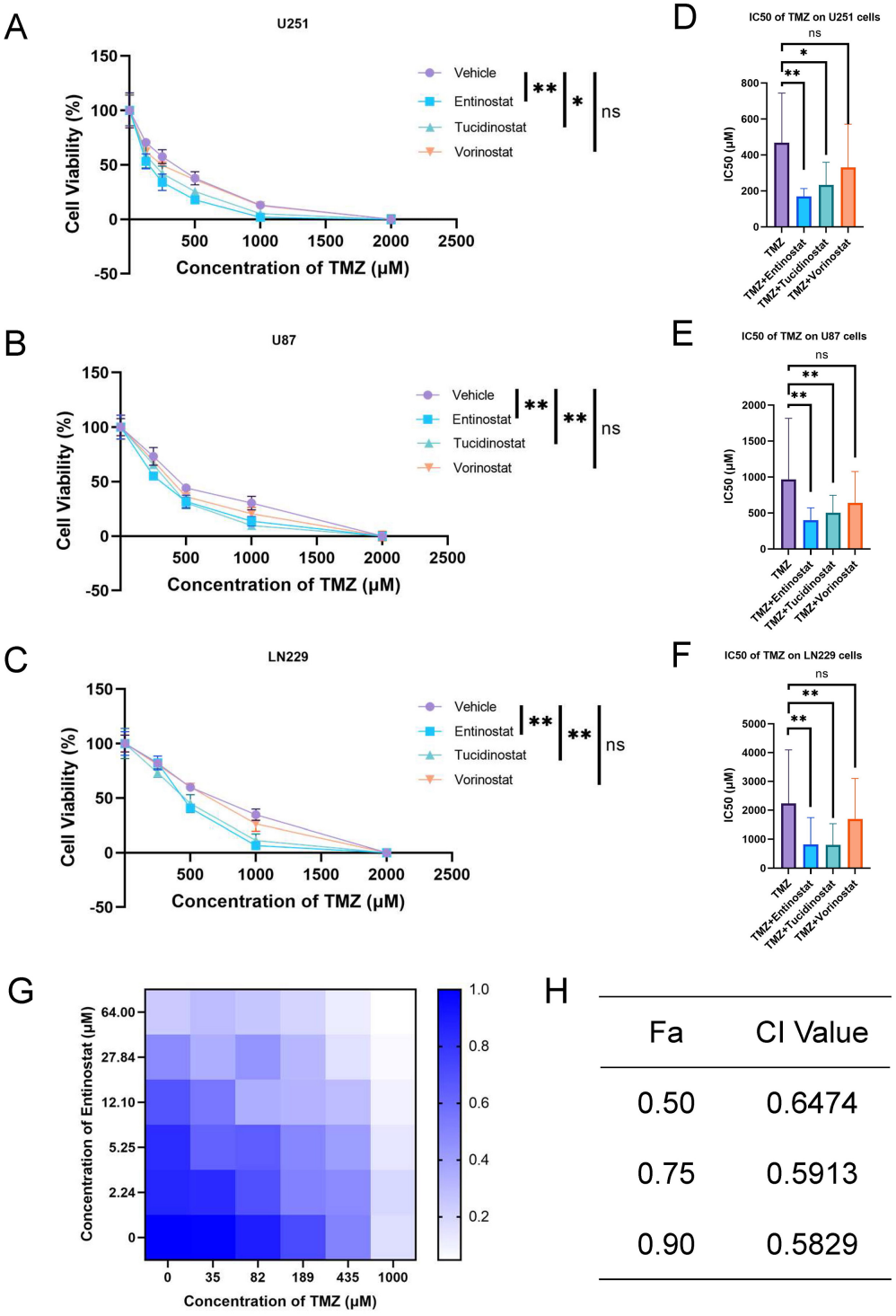

Fig. 1. HDAC inhibition potentiates TMZ-induced cytotoxicity in GBM cells. (A–C) Cell viability curves for U251 (A), U87 (B), LN229 (C) cells treated with increasing concentrations of TMZ alone or in combination with 1 μM HDAC inhibitors for 72 h. (D–F) Summary of TMZ IC_{50} values calculated from the viability curves of U251 (D), U87 (E) and LN229 (F). (G) Checkerboard analysis of the combinatorial effects of Entinostat and TMZ in U251 cells. The heatmap depicts normalized cell viability relative to untreated controls, with lighter colors indicating stronger growth inhibition under combination treatment. (H) Quantitative assessment of drug interaction between Entinostat and TMZ using the Chou–Talalay method. Values are presented as mean ± SEM from three independent experiments for panels A–C, while error bars in panels D–F represent the 95% confidence intervals. Statistical analysis was performed using two-way ANOVA for dose–response curves. Combination index (CI) values were calculated with CompuSyn software (Ver 1.0, ComboSyn Inc., Paramus, NJ, USA). * ($p < 0.05$), ** ($p < 0.01$), ns (not significant). TMZ, temozolomide; HDAC, histone deacetylase; GBM, glioblastoma; ANOVA, analysis of variance.

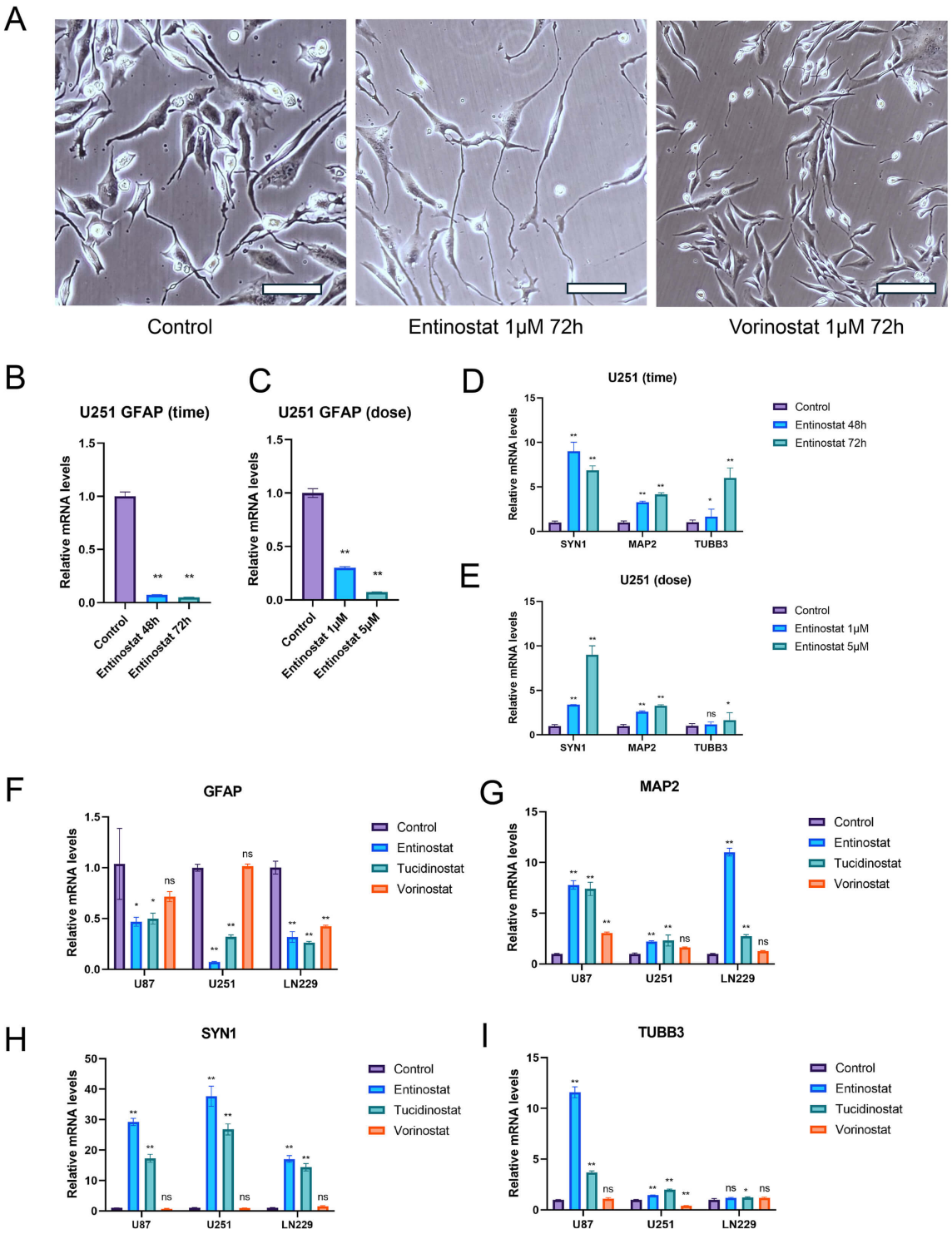

Fig. 2. Benzamide-class HDAC inhibitors are associated with selected marker and morphological changes in GBM cells. (A) Phase-contrast micrographs of U251 cells untreated (Control) or treated with 1 μM Entinostat or 1 μM Vorinostat for 72 h. Scale bars, 100 μm. (B,C) qRT-PCR analysis of GFAP in U251 cells treated with Entinostat at the indicated time points (B) and concentrations (C). (D,E) qRT-PCR analysis of SYN1, MAP2, and TUBB3 in U251 cells treated with Entinostat at the indicated time points (D) and concentrations (E). (F–I) qRT-PCR profiling of GFAP (F), MAP2 (G), SYN1 (H), and TUBB3 (I) in U87, U251, and LN229 cells following 72 h treatment with Entinostat, Tucidinostat, or Vorinostat. All qRT-PCR data were normalized to untreated controls and are presented as mean ± SEM from three independent experiments. Statistical analysis was performed using one-way ANOVA with Tukey's post-hoc test. * ($p < 0.05$), ** ($p < 0.01$), ns (not significant). GFAP, glial fibrillary acidic protein; WT, wild type; qRT-PCR, quantitative reverse transcription polymerase chain reaction; SYN1, synapsin I; MAP2, microtubule-associated protein 2; TUBB3, class III β-tubulin.

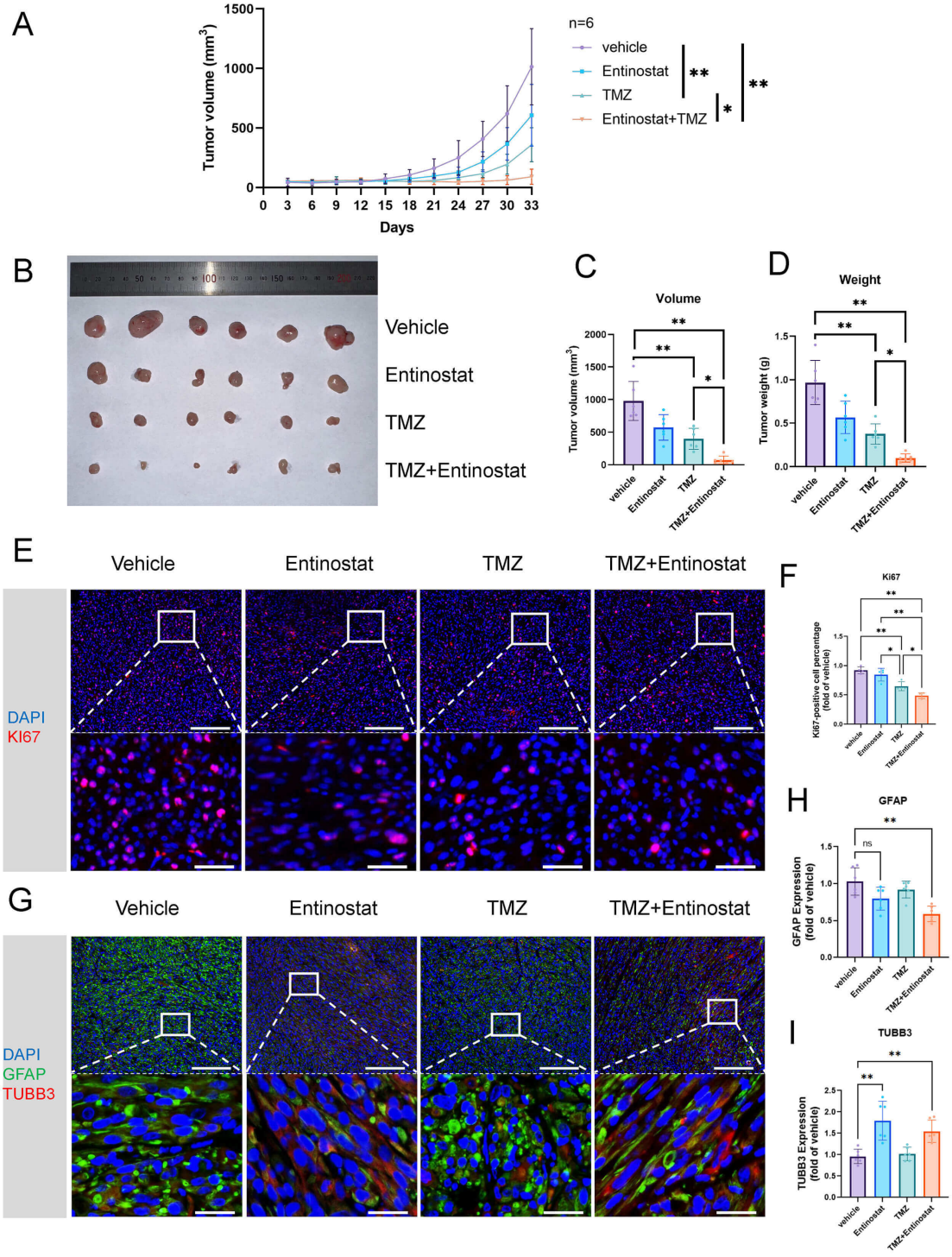

Fig. 3. Entinostat in combination with TMZ in a U87 xenograft model. (A) Tumor growth kinetics of subcutaneous U87 xenografts in BALB/c nude mice (n = 6 per group) treated with vehicle, Entinostat (5 mg/kg), TMZ (10 mg/kg), or Entinostat + TMZ combination therapy. Tumor volumes were measured every three days for 33 days. (B) Representative images of excised tumors at day 33. (C,D) Final tumor volumes (C) and weights (D). (E) Immunofluorescence staining of tumor sections for Ki67 (red); nuclei counterstained with DAPI (blue). Low-magnification images are shown with scale bars, 500 μm; enlarged views are shown with scale bars, 100 μm. (F) Quantification of Ki67-positive cell percentages from images in (E). (G) Immunofluorescence staining of tumor sections for GFAP (green), and TUBB3 (red); nuclei counterstained with DAPI (blue). Low-magnification images are shown with scale bars, 500 μm; enlarged views are shown with scale bars, 100 μm. (H,I) Quantification of mean fluorescence intensities for GFAP (H) and TUBB3 (I). Data are expressed as mean ± SEM. Statistical analyses were performed using two-way ANOVA for growth curves and one-way ANOVA with Tukey's post-hoc test for bar graphs. * ($p < 0.05$), ** ($p < 0.01$), ns (not significant). DAPI, 4',6-diamidino-2-phenylindole.

3.2 Entinostat and Tucidinostat Are Associated With Morphological and Marker Changes in GBM Cells

Visual inspection of Entinostat-treated GBM cells showed detectable morphological changes under the tested conditions. In U251 cells, exposure to 1 μM Entinostat for 72 h induced noticeable changes in cell morphology, including a more elongated appearance under the tested conditions (Fig. 2A). qRT-PCR analysis demonstrated a time- and dose-dependent downregulation of the astroglial marker glial fibrillary acidic protein (GFAP) (Fig. 2B,C), accompanied by altered expression of synapsin I (SYN1), microtubule-associated protein 2 (MAP2) and class III β-tubulin (TUBB3) (Fig. 2D,E). These transcriptional changes indicate altered expression of selected markers following treatment under the tested GBM conditions.

We next compared Entinostat, Tucidinostat, and Vorinostat across U87, U251, and LN229 cell lines. Both Entinostat and Tucidinostat significantly suppressed GFAP transcription and increased the expression of MAP2, TUBB3, and SYN1 in all tested lines (Fig. 2F–I). In contrast, Vorinostat failed to induce comparable morphological or transcriptional changes (Fig. 2A,F–I). Therefore, the marker and morphological changes were more pronounced with Entinostat and Tucidinostat than with Vorinostat under the tested conditions.

3.3 Entinostat Enhances TMZ Response in a U87 Xenograft Model

We next used a subcutaneous U87 xenograft model in BALB/c nude mice to test whether the chemosensitizing effect of Entinostat observed *in vitro* translates into sustained antitumor efficacy *in vivo*. During the initial three weeks post-implantation, TMZ monotherapy significantly suppressed tumor growth. However, its efficacy progressively diminished thereafter, consistent with the emergence of chemoresistant populations. Co-administration of Entinostat with TMZ produced strong and sustained inhibition of tumor growth throughout the entire treatment period (Fig. 3A). At study termination, tumors in the combination group exhibited markedly reduced volume and weight compared with all other treatment arms (Fig. 3B–D). Immunofluorescence staining revealed a lower Ki67 proliferation index in both TMZ-alone and combination groups relative to vehicle controls (Fig. 3E). Quantitative analysis confirmed the Ki67 index was significantly lower in the combination group compared to TMZ monotherapy (Fig. 3F), underscoring the chemosensitizing effect of Entinostat *in vivo*.

Based on the marker changes observed after Entinostat treatment *in vitro*, we subsequently examined GFAP and TUBB3 staining in xenograft tissues. Immunofluorescence staining revealed decreased GFAP and increased TUBB3 in tumors from Entinostat-treated mice (Fig. 3G), with quantification confirming statistical significance (Fig. 3H,I). Collectively, these *in vivo* results show that treatment with Entinostat plus TMZ was associated with sustained suppression of tumor growth in U87 xenografts, along with changes in GFAP and TUBB3 staining under the tested conditions.

3.4 HDAC1/2/3 Knockout Does Not Abolish Entinostat- or Tucidinostat-Associated TMZ Sensitization

To determine the role of individual Class I HDACs in the TMZ-sensitizing effects of benzamide-class inhibitors, we generated U251 and U87 cell lines with CRISPR-Cas9-mediated knockout of HDAC1, HDAC2, and HDAC3, as validated by Western blot (Fig. 4A). Compensatory upregulation of other HDAC family members could potentially account for the persistence of drug responses following Class I HDAC depletion. We therefore further examined the expression of representative HDACs from related subclasses, including the Class IIa enzymes HDAC4, HDAC5, HDAC7, and HDAC9, the Class IIb enzymes HDAC6 and HDAC10, and the Class I isoform HDAC8. qPCR analysis revealed no significant changes in the expression of these HDAC isoforms compared with wild-type (WT) controls (Fig. 4B), indicating that transcriptional upregulation of other related HDAC isoforms did not occur under the tested conditions. Triple knockout did not significantly affect baseline TMZ sensitivity. In WT cells, both Entinostat and Tucidinostat markedly enhanced TMZ efficacy (Fig. 4C–F), with substantial reductions in TMZ IC_{50} values (Fig. 4G,H, **Supplementary Table 4**). This sensitization was maintained in HDAC1/2/3 knockout (KO) cells. Combination treatment still reduced TMZ IC_{50} relative to TMZ alone, although the magnitude of change was smaller than in WT cells. These trends were consistent in viability curves. The above data indicate that canonical Class I HDAC inhibition is not solely responsible for Entinostat- and Tucidinostat-associated TMZ sensitization, and suggest that HDAC1/2/3 depletion did not fully account for the observed sensitization under these conditions.

3.5 Entinostat- and Tucidinostat-Associated Marker Changes Persist After HDAC1/2/3 Depletion

To investigate whether the observed marker changes depend on HDAC1/2/3, we examined marker expression in U251 and U87 HDAC1/2/3-KO cells treated with Entinostat or Tucidinostat. Notably, both agents were still associated with changes in GFAP, SYN1, MAP2, and TUBB3 expression in the KO background (Fig. 5A–H). These changes did not revert to baseline, despite the loss of HDAC1/2/3. Immunofluorescence staining corroborated these findings, revealing decreased GFAP, increased TUBB3, and morphological changes characteristic under the tested conditions in both WT and KO cells (Fig. 5I). Collectively, these results indicate the observed Entinostat- and Tucidinostat-associated marker changes were not abolished by HDAC1/2/3 knockout. Further studies are needed to determine the molecular basis and functional relevance of such changes.

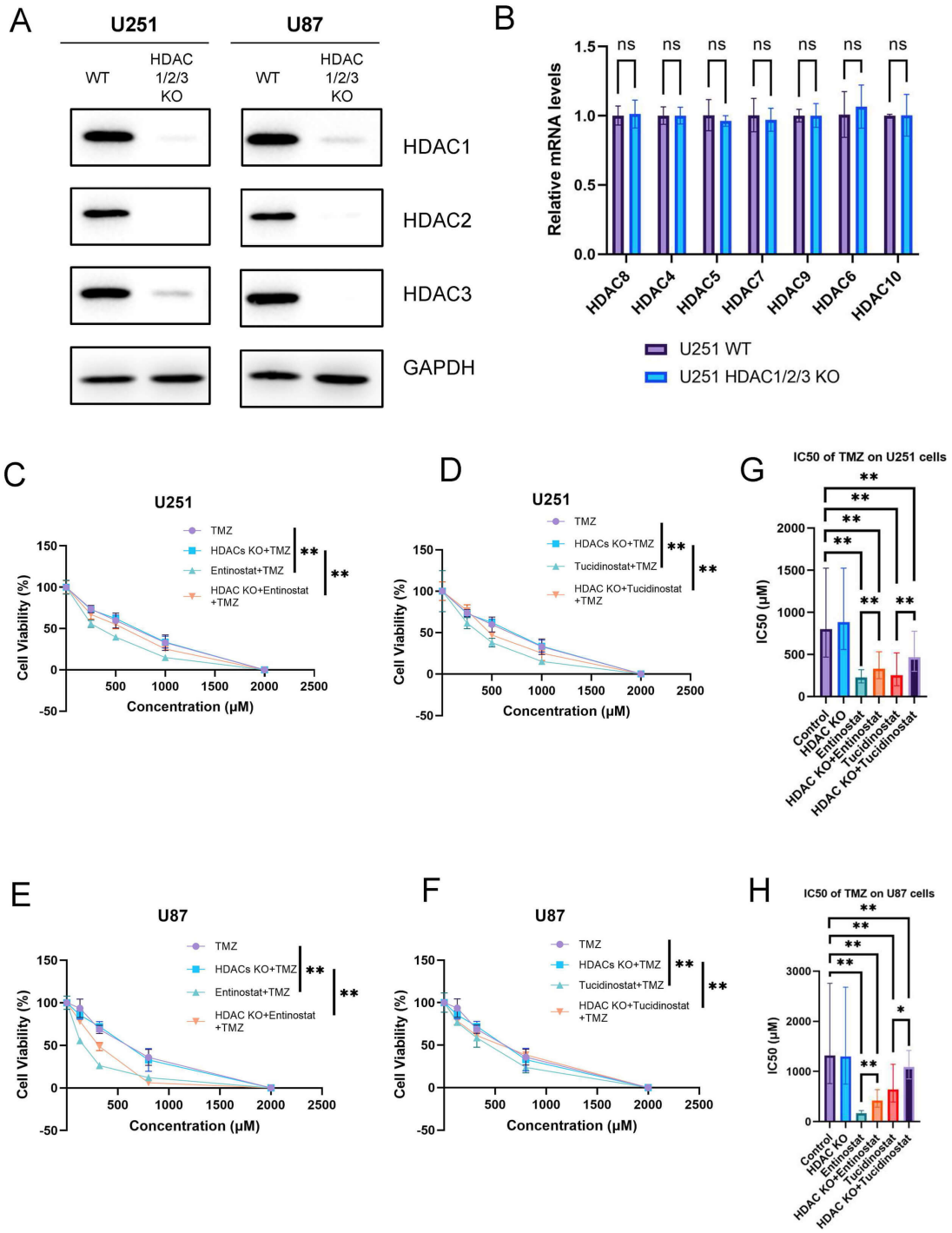

Fig. 4. Knockout of Class I HDACs and TMZ sensitivity in GBM cells. (A) Western blot validation of CRISPR-Cas9-mediated knockout of HDAC1, HDAC2, and HDAC3 in U251 and U87 cells; GAPDH served as a loading control. (B) Relative mRNA expression levels of HDAC4, HDAC5, HDAC6, HDAC7, HDAC8, HDAC9, and HDAC10 in WT and HDAC1/2/3 KO U251 cells. (C,D) Cell viability curves for U251 wild-type and HDAC1/2/3-knockout cells treated with increasing concentrations of TMZ alone or in combination with 1 μM Entinostat (C) or 1 μM Tucidinostat (D) for 72 h. (E,F) Cell viability curves for U87 wild-type and HDAC1/2/3-knockout cells treated with increasing concentrations of TMZ alone or in combination with 1 μM Entinostat (E) or 1 μM Tucidinostat (F) for 72 h. (G,H) Summary of TMZ IC_{50} values calculated from the viability curves of U251 (G) and U87 (H). Values are presented as mean ± SEM from three independent experiments for panels B–F, while error bars in panels G–H represent the 95% confidence intervals. Statistical analyses were performed using one-way ANOVA with Tukey's post hoc test. * ($p < 0.05$), ** ($p < 0.01$), ns (not significant). KO, knockout; GAPDH, glyceraldehyde-3-phosphate dehydrogenase; CRISPR-Cas9, Clustered Regularly Interspaced Short Palindromic Repeats associated protein 9.

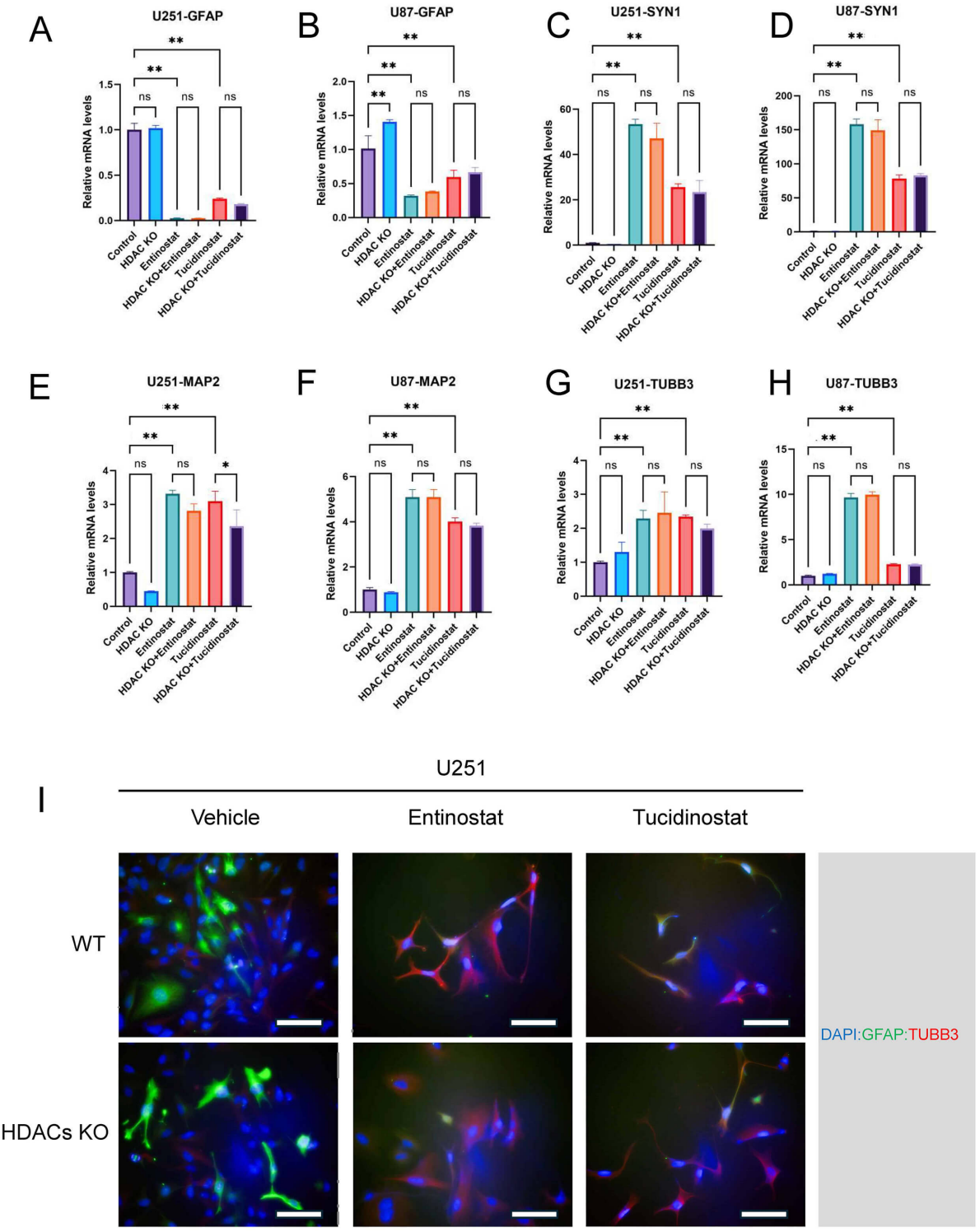

Fig. 5. Benzamide-class HDAC inhibitors are associated with marker and morphological changes in GBM cells with or without HDAC1/2/3 knockout. U251 and U87 wild-type and HDAC1/2/3-knockout cells following 72 h treatment with 1 μM Entinostat or 1 μM Tucidinostat. (A,B) qRT-PCR analysis of GFAP in U251 (A) and U87 (B) cells. (C,D) qRT-PCR analysis of SYN1 in U251 (C) and U87 (D) cells. (E,F) qRT-PCR analysis of MAP2 in U251 (E) and U87 (F) cells. (G,H) qRT-PCR analysis of TUBB3 in U251 (G) and U87 (H) cells. (I) Immunofluorescence images of U251 wild-type and HDAC1/2/3-knockout cells treated with vehicle, Entinostat, or Tucidinostat for 72 h. GFAP (green), TUBB3 (red), and nuclei (DAPI, blue) were visualized. Scale bars, 100 μm. Data are presented as mean ± SEM from three independent experiments. Statistical significance was determined using one-way ANOVA with Tukey's post hoc test. * ($p < 0.05$), ** ($p < 0.01$), ns (not significant).

4. Discussion

TMZ resistance remains a major obstacle to durable therapeutic responses in GBM, largely driven by epigenetically regulated DNA damage tolerance pathways. This study examined the effects of Entinostat and Tucidinostat on the response to TMZ in GBM models. Contrary to the prevailing assumption that sensitization is solely mediated through Class I HDAC suppression [12,20], CRISPR-Cas9-mediated knockout of HDAC1, HDAC2, and HDAC3 did not alter baseline TMZ sensitivity, and yet Entinostat and Tucidinostat retained their sensitizing capacity in knockout cells. The chemosensitizing effects and associated marker changes persisted in HDAC1/2/3-knockout cells. This is a significant finding that suggests canonical Class I HDAC inhibition alone may not fully explain the biological effects of Entinostat and Tucidinostat, raising the possibility that additional mechanisms may contribute to TMZ sensitization. Further mechanistic studies will be required to determine the molecular basis of these effects.

This work also found that Entinostat and Tucidinostat were associated with changes in the expression of selected markers and in the morphology of GBM cells. These changes persisted despite CRISPR-Cas9-mediated depletion of HDAC1/2/3, suggesting that HDAC1/2/3 depletion alone does not fully account for the observations made in the present models. The molecular basis for these observations remains unclear. Decreased GFAP and increased MAP2 and TUBB3 expression levels were observed after treatment, but the functional meaning of these changes remains unclear. In solid tumors, altered TUBB3 expression has been reported in association with treatment response and cellular stress [25]. Treatment with HDAC inhibitor may alter transcriptional programs associated with the selected markers examined here [26,27]. The observed changes in markers may be associated with reduced tumor-cell proliferation under the tested conditions, although causality remains to be established. Importantly, the changes should not be interpreted as evidence of neuronal differentiation, neuronal transdifferentiation, or stable lineage conversion. Although MAP2, TUBB3, and SYN1 are commonly associated with neuronal or cytoskeletal programs, the current study did not assess electrophysiological maturation, synaptic function, lineage conversion, or long-term neuronal identity. The persistence of these effects after HDAC1/2/3 knockout suggests that additional mechanisms may contribute to the observed changes, although their identity and therapeutic relevance remain to be determined. Additional mechanistic studies may clarify the molecular basis of these observations.

Taken together, our findings suggest that Entinostat and Tucidinostat may enhance the response to TMZ in the present GBM models through mechanisms not fully explained by HDAC1/2/3 depletion. Compared with the hydroxamic acid-based pan-HDAC inhibitor Vorinostat, Entinostat and Tucidinostat demonstrated more consistent TMZ-sensitizing activity across multiple GBM cell lines. Furthermore, while the subcutaneous U87 xenograft model provides valuable initial proof-of-concept for the *in vivo* efficacy of this combination, it does not fully recapitulate the complex, immune-competent, and highly invasive microenvironment of human GBM. Therefore, future studies utilizing orthotopic and syngeneic GBM models are essential to more thoroughly evaluate the true translational and clinical potential of this therapeutic strategy. Future work should assess the reversibility and functional relevance of the observed morphological and marker changes.

5. Conclusion

In summary, our findings demonstrate that Entinostat and Tucidinostat sensitized GBM models to TMZ more consistently than Vorinostat under the conditions tested. In addition to potentiating TMZ-induced cytotoxicity, these compounds were associated with changes in the expression of selected markers and in the cell morphology of GBM cells. Critically, both chemosensitization and these effects were not abolished by HDAC1/2/3 knockout, suggesting that HDAC1/2/3 depletion alone does not fully explain the observed responses under the tested conditions. The present findings support continued investigation of Entinostat and Tucidinostat as combination partners for TMZ in GBM models.

Availability of Data and Materials

The datasets generated and analyzed during the current study are available from the corresponding author upon reasonable request.

Author Contributions

RC and QL designed the research study. RC, JS, XD, XT, and YY performed the experiments and collected the data. RC analyzed the data and drafted the manuscript. JS, XD, XT, and YY contributed to data interpretation and manuscript revision. QL supervised the study, provided critical guidance throughout the project, and revised the manuscript. All authors contributed to editorial changes in the manuscript, read and approved the final version of the manuscript. All authors have participated sufficiently in the work and agreed to be accountable for all aspects of the work.

Ethics Approval and Consent to Participate

All animal care and experimental procedures were conducted in accordance with the relevant guidelines and regulations, and were approved by the Experimental Animal Ethics Committee of Fudan University (Approval No.: 2025-02-YL-LQQ-03). The study was designed and reported in accordance with the ARRIVE 2.0 guidelines and the Chinese National Standard GB/T 35892–2018 (Guideline for Ethical Review of Animal Welfare).

Acknowledgment

Not applicable.

Funding

This research received no external funding.

Conflicts of Interest

The authors declare no conflicts of interest.

Declaration of AI and AI-Assisted Technologies in the Writing Process

During the preparation of this manuscript, the authors used ChatGPT strictly for the purpose of language polishing, grammar checking, and improving the readability of the English text. The AI tool was not used for data generation, analysis, or drawing scientific conclusions. After using this tool, the authors thoroughly reviewed and edited the output as necessary and take full and sole responsibility for the entire content of the published work.

Supplementary Material

Supplementary material associated with this article can be found, in the online version, at https://doi.org/10.31083/Pharmazie51570.

References

[1] Chen R, Smith-Cohn M, Cohen AL, Colman H. Glioma Subclassifications and Their Clinical Significance. Neurotherapeutics: the Journal of the American Society for Experimental NeuroTherapeutics. 2017; 14: 284–297. https://doi.org/10.1007/s13311-017-0519-x

[2] Louis DN, Perry A, Reifenberger G, von Deimling A, Figarella-Branger D, Cavenee WK, et al. The 2016 World Health Organization Classification of Tumors of the Central Nervous System: a summary. Acta Neuropathologica. 2016; 131: 803–820. https://doi.org/10.1007/s00401-016-1545-1

[3] Louis DN, Perry A, Wesseling P, Brat DJ, Cree IA, Figarella-Branger D, et al. The 2021 WHO Classification of Tumors of the Central Nervous System: a summary. Neuro-oncology. 2021; 23: 1231–1251. https://doi.org/10.1093/neuonc/noab106

[4] Johnson DR, O'Neill BP. Glioblastoma survival in the United States before and during the temozolomide era. Journal of Neuro-oncology. 2012; 107: 359–364. https://doi.org/10.1007/s11060-011-0749-4

[5] Weller M, van den Bent M, Preusser M, Le Rhun E, Tonn JC, Minniti G, et al. EANO guidelines on the diagnosis and treatment of diffuse gliomas of adulthood. Nature Reviews. Clinical Oncology. 2021; 18: 170–186. https://doi.org/10.1038/s41571-020-00447-z

[6] Stupp R, Mason WP, van den Bent MJ, Weller M, Fisher B, Taphoorn MJB, et al. Radiotherapy plus concomitant and adjuvant temozolomide for glioblastoma. The New England Journal of Medicine. 2005; 352: 987–996. https://doi.org/10.1056/NEJMoa043330

[7] Jezierzański M, Nafalska N, Stopyra M, Furgoł T, Miciak M, Kabut J, et al. Temozolomide (TMZ) in the Treatment of Glioblastoma Multiforme-A Literature Review and Clinical Outcomes. Current Oncology (Toronto, Ont.). 2024; 31: 3994–4002. https://doi.org/10.3390/curroncol31070296

[8] Filley AC, Henriquez M, Dey M. Recurrent glioma clinical trial, CheckMate-143: the game is not over yet. Oncotarget. 2017; 8: 91779–91794. https://doi.org/10.18632/oncotarget.21586

[9] Tan AC, Ashley DM, López GY, Malinzak M, Friedman HS, Khasraw M. Management of glioblastoma: State of the art and future directions. CA: a Cancer Journal for Clinicians. 2020; 70: 299–312. https://doi.org/10.3322/caac.21613

[10] Cavalli G, Heard E. Advances in epigenetics link genetics to the environment and disease. Nature. 2019; 571: 489–499. https://doi.org/10.1038/s41586-019-1411-0

[11] Kondo Y, Katsushima K, Ohka F, Natsume A, Shinjo K. Epigenetic dysregulation in glioma. Cancer Science. 2014; 105: 363–369. https://doi.org/10.1111/cas.12379

[12] Wu Q, Berglund AE, Etame AB. The Impact of Epigenetic Modifications on Adaptive Resistance Evolution in Glioblastoma. International Journal of Molecular Sciences. 2021; 22: 8324. https://doi.org/10.3390/ijms22158324

[13] Hegi ME, Diserens AC, Gorlia T, Hamou MF, de Tribolet N, Weller M, et al. MGMT gene silencing and benefit from temozolomide in glioblastoma. The New England Journal of Medicine. 2005; 352: 997–1003. https://doi.org/10.1056/NEJMoa043331

[14] Oldrini B, Vaquero-Siguero N, Mu Q, Kroon P, Zhang Y, Galán-Ganga M, et al. MGMT genomic rearrangements contribute to chemotherapy resistance in gliomas. Nature Communications. 2020; 11: 3883. https://doi.org/10.1038/s41467-020-17717-0

[15] Tian X, Liu G, Ji L, Shen Y, Gu J, Wang L, et al. Histone-acetyl epigenome regulates TGF-β pathway-associated chemoresistance in colorectal cancer. Translational Oncology. 2025; 51: 102166. https://doi.org/10.1016/j.tranon.2024.102166

[16] Debbarma M, Sarkar K, Sil SK. Dissecting the epigenetic orchestra of HDAC isoforms in breast cancer development: a review. Medical Oncology (Northwood, London, England). 2024; 42: 1. https://doi.org/10.1007/s12032-024-02553-9

[17] Beumer JH, Tawbi H. Role of histone deacetylases and their inhibitors in cancer biology and treatment. Current Clinical Pharmacology. 2010; 5: 196–208. https://doi.org/10.2174/157488410791498770

[18] Garmpis N, Damaskos C, Dimitroulis D, Kouraklis G, Garmpi A, Sarantis P, et al. Clinical Significance of the Histone Deacetylase 2 (HDAC-2) Expression in Human Breast Cancer. Journal of Personalized Medicine. 2022; 12: 1672. https://doi.org/10.3390/jpm12101672

[19] Grinshtein N, Rioseco CC, Marcellus R, Uehling D, Aman A, Lun X, et al. Small molecule epigenetic screen identifies novel EZH2 and HDAC inhibitors that target glioblastoma brain tumor-initiating cells. Oncotarget. 2016; 7: 59360–59376. https://doi.org/10.18632/oncotarget.10661

[20] Hanisch D, Krumm A, Diehl T, Stork CM, Dejung M, Butter F, et al. Class I HDAC overexpression promotes temozolomide resistance in glioma cells by regulating RAD18 expression. Cell Death & Disease. 2022; 13: 293. https://doi.org/10.1038/s41419-022-04751-7

[21] Lo Cascio C, Margaryan T, Luna-Melendez E, McNamara JB, White CI, Knight W, et al. Quisinostat is a brain-penetrant radiosensitizer in glioblastoma. JCI Insight. 2023; 8: e167081. https://doi.org/10.1172/jci.insight.167081

[22] Sun Y, Sun Y, Yue S, Wang Y, Lu F. Histone Deacetylase Inhibitors in Cancer Therapy. Current Topics in Medicinal Chemistry. 2018; 18: 2420–2428. https://doi.org/10.2174/1568026619666181210152115

[23] Roche J, Bertrand P. Inside HDACs with more selective HDAC inhibitors. European Journal of Medicinal Chemistry. 2016; 121: 451–483. https://doi.org/10.1016/j.ejmech.2016.05.047

[24] Ran FA, Hsu PD, Wright J, Agarwala V, Scott DA, Zhang F. Genome engineering using the CRISPR-Cas9 system. Nature

Protocols. 2013; 8: 2281–2308. https://doi.org/10.1038/nprot.2013.143

[25] Duly AMP, Kao FCL, Teo WS, Kavallaris M. βIII-Tubulin Gene Regulation in Health and Disease. Frontiers in Cell and Developmental Biology. 2022; 10: 851542. https://doi.org/10.3389/fcell.2022.851542

[26] Marampon F, Megiorni F, Camero S, Crescioli C, McDowell HP, Sferra R, et al. HDAC4 and HDAC6 sustain DNA double strand break repair and stem-like phenotype by promoting radioresistance in glioblastoma cells. Cancer Letters. 2017; 397: 1–11. https://doi.org/10.1016/j.canlet.2017.03.028

[27] Zhao S, Zhao R, Wang C, Ma C, Gao Z, Li B, et al. HDAC7 drives glioblastoma to a mesenchymal-like state via LGALS3-mediated crosstalk between cancer cells and macrophages. Theranostics. 2024; 14: 7072–7087. https://doi.org/10.7150/thno.100939